Characteristic and Performance of Ni, Pt, and Pd Monometal and Ni-Pd Bimetal onto KOH Activated Carbon for Hydrotreatment of Castor Oil

Wega Trisunaryanti*, Triyono Triyono, Iip Izul Falah, Dwi Bagus Wicaksono, and Satriyo Dibyo Sumbogo

Department of Chemistry, Faculty of Mathematics and Natural Sciences, Universitas Gadjah Mada, Sekip Utara, Yogyakarta 55281, Indonesia

** **Corresponding author:***

email: wegats@ugm.ac.id

Received: May 21, 2023
Accepted: September 7, 2023

DOI: 10.22146/ijc.84640

Abstract: *The preparation of highly efficient hydrotreating catalysts has presented a significant challenge in the field of catalysis. In this study, chemically activated carbon (AC) was prepared using potassium hydroxide (KOH) as an activator and Merbau wood as a lignocellulosic source for the AC. The AC was then impregnated with mono-metallic species (nickel, platinum, and palladium) as well as a bimetallic NiPd combination. The results revealed that the optimal KOH impregnation weight ratio was determined to be 2:1, resulting in a remarkably high iodine value of 751.94 mg/g. Subsequently, AC was employed as a support material for the hydrotreating of castor oil. Among the catalysts tested, the NiPd/AC catalyst demonstrated superior performance, yielding a liquid fraction comprising 88.80 wt.%. Within this fraction, C5-C12 hydrocarbons accounted for 15.16 wt.%, alcohol compounds constituted 71.69 wt.%, while the remaining 0.87 wt.% consisted of other components. Furthermore, the NiPd/AC catalyst exhibited remarkable stability, as its performance remained largely unchanged even after being used three times consecutively. This finding suggests that coking had minimal impact on the active sites of the mentioned catalyst, indicating its robustness and potential for prolonged application.*

Keywords: *biofuels; activated carbon; hydrotreating; castor oil*

■ INTRODUCTION

The depletion of crude oil reserves and the escalating global fuel consumption have become pressing concerns [1-2]. The Energy Information Administration (EIA) projects a substantial 71% increase in fuel consumption worldwide from 2000 to 2030, highlighting the urgent need for alternative energy sources to replace fossil fuels [3-4]. Hydrotreated non-edible vegetable oils hold significant potential as renewable energy sources that can effectively replace fossil fuels, given their abundant triglyceride content that can be converted into hydrocarbons [5-10]. Unlike FAME biofuels, the hydrocarbons produced through this process closely resemble those derived from fossil fuels, making the hydrotreatment of vegetable oils highly promising for contemporary vehicular applications [11-13]. Castor oil emerges as a strong candidate due to its exceptionally high ricinoleic acid content, ranging from 75 to 95% [14-15]. However, the presence of hydroxyl groups in castor oil poses a challenge in the hydrotreating process, making its conversion into hydrocarbons more difficult. Therefore, the use of catalysts with superior hydrodeoxygenation (HDO) performance is imperative for this task [16].

Sulfided catalysts are commonly employed for the HDO of vegetable oils, but this type of catalyst necessitates an additional step of sulfur removal during the sulfidation process. Unfortunately, sulfur removal negatively affects the HDO process of vegetable oils. Therefore, there is a preference for non-sulfided catalysts [11]. To address this challenge, mono- and bimetallic catalysts have been successfully utilized for the hydrotreatment of vegetable oils [17-19]. Palladium (Pd) metal possesses unique properties in the hydrotreating process, such as its ability to adsorb more

hydrogen than other metals through an overspill mechanism. However, its high cost limits its application to low concentrations [20]. Another more cost-effective option is monometallic nickel (Ni), which has been proven capable of hydrocracking and HDO applications for various vegetable oils in previous studies [21-23]. To prevent aggregation and preserve the active surface area, it is essential to support the transition metal with a suitable support material [24]. For the hydrotreating of castor oil, the support material needs to possess high surface area, thermal stability, and sufficient acidity.

Activated carbon is a viable choice as a support material due to its adjustable porosity, which can be controlled through various synthesis and preparation methods [25]. Chemicals such as H_3PO_4, H_2O_2, and Na_2CO_3 are often used in activating the carbon material [26-28]. However, the utilization of KOH as the activation chemical in the chemical activation method offers notable advantages, as it has been experimentally proven to generate well-developed microporosity and a high surface area [29-31]. The microporous characteristics of the material can be finely tuned by adjusting the impregnation ratio of KOH, thereby achieving the highest surface area primarily dominated by a microporous structure [29]. It is important to note that although a microporous support material provides a large surface area, the presence of small pores imposes diffusion limitations on the feed molecules, particularly considering their large molecular size, which necessitates initial cracking. Consequently, the catalyst becomes more prone to coking [22, 32]. Moreover, there is a limited understanding of the synergistic behavior exhibited by mono- and bimetallic catalysts supported on microporous activated carbon in hydrotreating applications.

This study aimed to investigate the optimal KOH impregnation ratio for achieving the maximum surface area using Merbau wood as a lignocellulosic source. Furthermore, the synergistic behavior between mono- and bimetallic catalysts supported on a microporous support material was examined for their effectiveness as catalysts in the hydrotreatment of castor oil. Additionally, the reusability of the catalysts was investigated, considering the propensity of microporous supports for coking.

■ EXPERIMENTAL SECTION

Materials

The waste woods used in this research were obtained from Manokwari, Papua Barat. The castor oil used for hydrotreatment was obtained from the local store. Acetone, hydrochloric acid, and KOH were analytical grade and purchased from Merck. $AgNO_3$, $Ni(NO_3)_2{\cdot}6H_2O$, $PdCl_2$, and $PtCl_4$ were supplied by Merck and used without further purification. The gases used in this research (i.e., H_2, and N_2) were supplied by PT Surya Indotim Imex.

Instrumentation

The instrumentations used in this study were infrared spectroscopy (Shimadzu Prestige 21), SEM-EDX mapping (SEM, JEOL JSM-6510LA), surface area analyzer (QuadraSorb Station 2), gas chromatography-mass spectrometry (Shimadzu QP2010S), and X-Ray diffraction spectroscopy (XRD6000, Shimadzu).

Procedure

Synthesis of activated carbon

As much as 60 g of Merbau wood was dried at 100 °C for 24 h. The dried wood was then crushed and sieved before being calcined into char with the furnace at 800 °C for 2 h under N_2 gas flow of 20 mL/min. The synthesized char was then washed using acetone in Soxhlet for 25 cycles and dried in an oven at 100 °C for 24 h. This material is then marked as C.

Subsequently, the dried material A was subjected to a mixing process with solid KOH at varying weight ratios of material A to KOH (C/KOH) - specifically, 1, 2, 3, and 4. The resulting mixture was then subjected to calcination at a temperature of 800 °C for a duration of 1 h under a controlled nitrogen gas flow of 20 mL/min. Following calcination, the resulting calcined materials were subjected to washing with a 2.0 M HCl solution at a temperature of 60 °C for 3 h. Subsequently, the washed materials were neutralized through treatment with demineralized water and subsequently dried in an oven at 100 °C for 24 h.

The activated carbon (AC) samples obtained through this rigorous purification process were then

designated as AC1, AC2, AC3, and AC4 based on the corresponding weight ratios employed during the preparation. Among these samples, AC material with the highest iodine value, signifying its superior adsorption capacity, was selected as the preferred support material for subsequent metal impregnation procedures.

Metal impregnation onto AC

To initiate the impregnation procedure, a precise amount of 37.155 mg of $Ni(NO_3)_2{\cdot}6H_2O$ was accurately weighed and added to a water solution containing 3.00 g of AC using the wet impregnation method. The impregnation process involved mixing the metal salt and the support material for 24 h, followed by solvent evaporation at 100 °C until complete removal of the solvent was achieved. Subsequently, the resulting impregnated materials were subjected to calcination at 550 °C under a controlled flow of H_2 gas at a rate of 20 mL/min.

Similarly, the synthesis of Pd/AC and Pt/AC catalysts was performed using 15.25 mg (0.3 wt.%) and 15.54 mg (0.3 wt.%) of the corresponding salt precursors, respectively. For the production of the bimetallic catalyst Ni-Pd/AC, a precise amount of 37.155 mg of $Ni(NO_3)_2{\cdot}6H_2O$ and 15.25 mg of $PdCl_2$ were dispersed into a solution containing 3.00 g of AC, facilitating the synthesis of the desired bimetallic catalyst.

Catalyst characterization

Functional groups in the char and AC were characterized by Fourier transform infrared spectroscopy. The morphology of the char, AC, Co/AC, Ni/AC, and Pd/AC were characterized and analyzed by using SEM-EDX mapping. The amorphous phase of AC and the crystalline phases of the metals were characterized by using XRD. The porosity of the catalysts was tested by using a surface area analyzer.

Hydrotreatment of castor oil

Catalyst performance testing was done in a semi-fixed batch reactor under the flow of hydrogen gas. The catalyst was placed in a stainless-steel holder above the feed with the ratio between the catalyst and the feed is 1:100. Hydrotreatment was done for 2 h at the temperature of 550 °C under the flow of hydrogen gas of 20 mL/min. The product obtained from the hydrotreatment process was then analyzed using GC-MS. Gasoline and diesel fraction is defined as hydrocarbon compound that has a carbon number of C4-C12 and C13-C20, respectively. Alcohol fraction is defined as an alcohol compound having any carbon number, and others are defined as any other compounds besides hydrocarbon and alcohol as shown in Eq. (1)-(7);

$$\text{Residue} = \frac{W_R}{W_F} \times 100\% \quad (1)$$

$$\text{Liquid fraction(wt.\%)} = \frac{W_P}{W_F} \times 100\% \quad (2)$$

$$\text{Coke} = \frac{W_{C2} - W_{C1}}{W_F} \times 100\% \quad (3)$$

$$\text{Gas} = 100\% - (\text{liquid fraction} + \text{coke} + \text{residue}) \quad (4)$$

$$\text{Gasoline} = (\%\ \text{Area of}\ C_5\text{–}C_{12}) \times \text{liquid fraction} \quad (5)$$

$$\text{Diesel oil} = (\%\ \text{Area of}\ C_{13}\text{–}C_{20}) \times \text{liquid fraction} \quad (6)$$

$$\text{OLP fraction} = \text{liquid fraction} - (\text{gasoline} - \text{diesel oil}) \quad (7)$$

where W_R = weight of unconverted feed, W_F = weight of the feed, W_{C1} = weight of the catalyst before hydrotreatment, and W_{C2} = weight of the catalyst after hydrotreatment. The reusability test was done on the same catalyst without any preparation for the used catalyst.

■ RESULTS AND DISCUSSION

Synthesis of Activated Carbon

The effect of KOH:C ratio on its iodine value is presented in Fig. 1. The iodine value was used to compare the resulting AC because its value is proportional to the total surface area. It could be seen that the ratio of 2:1 is the optimal ratio for activating the Merbau Wood, as its iodine value was 751.94 mg/g. In this ratio, the pore formation could be maximized without destroying the carbon material. The pore formation was caused by the breakdown of the ester bond from the lignin by KOH. During the activation process, the impregnated KOH decomposed into inorganic K, which helps the formation of pore structure. On the other hand, the ratio above 2:1 showed a gradual decrease in iodine value, which indicates structural collapse might have occurred in the high ratio

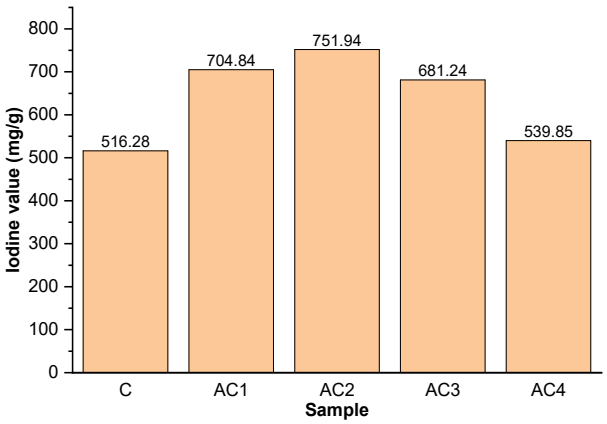

Fig 1. The iodine value of Char (C) and Activated Cabon (AC1, AC2, AC3, and AC4)

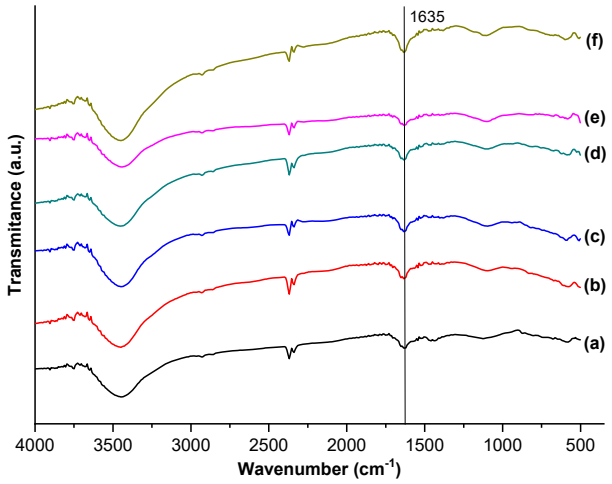

Fig 2. FTIR spectra of (a) C, (b) AC, (c) Ni/AC, (d) Pt/AC, (e) Pd/AC, and (f) NiPd/AC catalyst

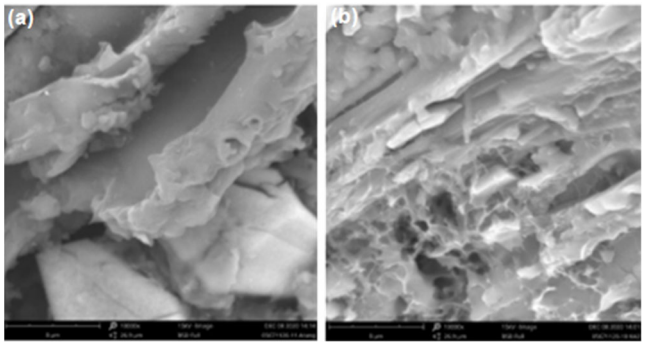

Fig 3. SEM image of (a) C and (b) AC2

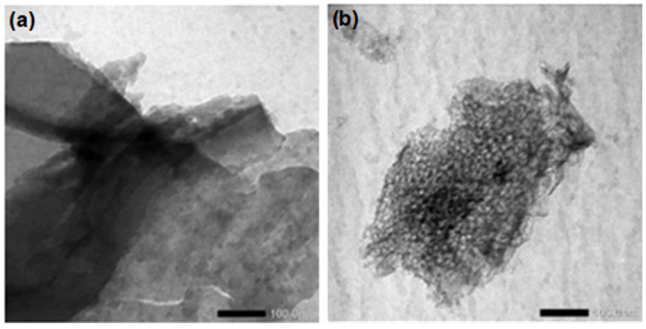

Fig 4. TEM image of (a) C and (b) AC2

of KOH:C, which is also seen in previous study on high ratio [29]. Therefore, AC2 was chosen to be further analyzed, characterized, and impregnated with metal in the next step.

The functional groups of C and AC2 are shown in Fig. 2. The KOH activation alters the carbon functional group, but only its backbone. The formation of aromatic carbon, C=C, was observed at 1635 cm^{-1}, implying that the activation process convert the biomass into a graphitic structure, as explained by a previous study by another group [33]. This functional group gives more hydrophobic AC. No significant changes of intensity regarding the hydroxyl group at 3445 cm^{-1} or any new functional groups were observed in spectral data.

Microstructures from SEM images of C and AC2 are shown in Fig. 3. The activation process using KOH caused the wall structure of the carbon to be thinner and more perforated. The nanostructure from the TEM image of C and AC2, shown in Fig. 4**,** also portrays a more perforated and thinner wall structure of the carbon after the activation process. More open pore structure gives easier access for the adsorbate to enter the AC through enhanced diffusion [34]. The perforation of the wall structure occurred due to the breakdown of the ester bond from the lignin.

The effect of the perforating process during activation was causing growth to the carbon pore properties, such as pore diameter, surface, and volume, presented in Table 1. These data are in good agreement with our previous study, where newly formed pores increased the carbon porosity properties [22]. The N_2 adsorption-desorption isotherm of C and AC is presented in Fig. 5. The carbon material prior to the activation was found to be of type III of IUPAC classification, which describes macroporous material that has weak adsorbate-adsorbent interaction. Activation with KOH that creates many micropores shifted the adsorption-desorption nature of the carbon into type IV isotherm, which describes micro-mesoporous

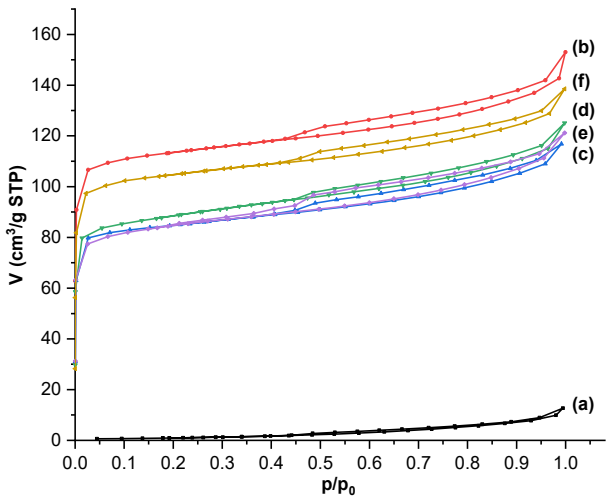

Fig 5. Isotherm graph of (a) C, (b) AC, (c) Ni/AC, (d) Pt/AC, (e) Pd/AC, and (f) NiPd/AC catalyst

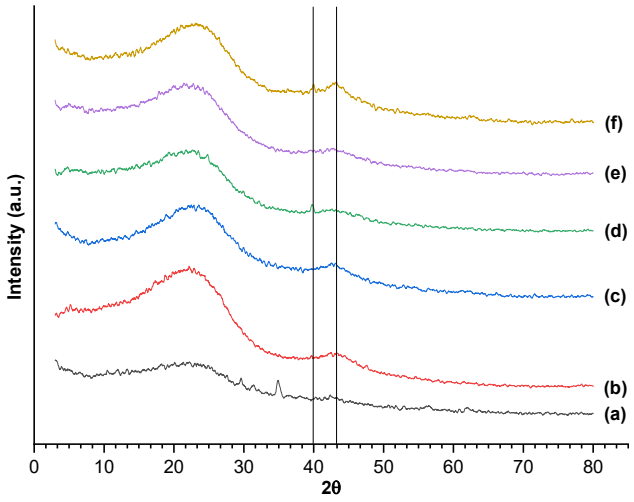

Fig 6. Diffractogram of (a) C, (b) AC, (c) Ni/AC, (d) Pt/AC, (e) Pd/AC, and (f) NiPd/AC catalyst

Table 1. Physical and chemical properties of the catalyst

Materials	Metal content (wt.%)			Acidity	S_{BET}	V_{pore}	Average pore
	Ni	Pt	Pd	(mmol/g)	(m^2/g)	(cm^3/g)	diameter (nm)
C	-	-	-	3.52	4.35	0.018	3.99
AC	-	-	-	3.92	469.86	0.225	2.25
Ni/AC	4.94	-	-	4.29	353.10	0.180	2.28
Pt/AC	-	0.37	-	4.79	341.40	0.185	2.26
Pd/AC	-	-	0.42	4.99	351.80	0.190	2.62
NiPd/AC	3.26	-	0.27	5.12	428.50	0.210	2.22

material. The thin body hysteresis indicates low mesopore volume compared to the low p/p_0 region contribution, which indicates the presence of micropores.

The diffractogram of both materials is shown in Fig. 6. Although both materials are amorphous, it seems that the activation process using KOH altered the carbon crystallinity, as the AC has better crystallinity compared to the char. Better crystallinity was caused by the formation of graphitic structure across the carbon amorphous matrix. The graphitic structure is also confirmed by its functional group, C=C, as discussed earlier in the FTIR section. Based on the discussed data, it can be deduced that the AC porous material was successfully synthesized.

Metal Impregnation

The impregnated metal inside the catalyst gives its own unique diffractogram peak, as shown in Fig. 6. Based on the additional peaks that exist in the diffractogram, all the impregnated metals are present in their reduced form, except for Pt/AC, which does not give an additional peak. The additional peak of Ni metal at 2θ 43.28° is attributed to the (111) plane of Ni (ICDD No. 00-045-1027). The Pd metal additional peak showed at 2θ 40.02° attributed to the (111) plane of Pd (ICDD No. 01-087-0637). Both Ni and Pd peaks can be observed in NiPd/AC catalyst. The absence of Pt metal additional peak could be caused by the small size of the amorphous impregnated Pt metal [16].

Although Pt metal was not observed in the diffractogram, the presence of Pt metal can be detected and analyzed using SEM-EDX. The Pt metal is presumed to exhibit excellent dispersion within the support material, resulting in the absence of any detectable crystal structure, at least within the limit of XRD detection. The content of the impregnated metal is shown in Table 1. The differences between the added metal concentration and the metal that is present in the

catalyst could be caused by the heterogeneity of metal dispersion and possibly metal aggregation across the AC matrix.

The adsorption-desorption isotherm graph from each catalyst is presented in Fig. 5. All the catalysts showed type IV adsorption isotherm with an H4 pattern for the hysteresis. Although they shared the same type of adsorption isotherm and hysteresis type, the NiPd/AC catalyst has the highest N_2 adsorption after the AC, as can be seen in Fig. 5. The low relative pressure region of the NiPd/AC has the highest slope among the other metal-impregnated catalysts, which indicates that the micropore is not blocked. This could be caused by the good metal dispersion of the Ni and Pd bimetal system, which does not block micropores in the catalyst.

The specific surface area of the catalyst is presented in Table 1. The NiPd/AC catalyst shows the slightest decrease among the other impregnated metal catalysts in terms of the specific surface area and pore volume. This result is in alignment with the isotherm data where the NiPd/AC catalyst is suspected to have an unblocked micropores region and rather good bimetal dispersion compared to the other impregnated catalyst. This argument is also proven by its TEM image, where the metals seem to be evenly distributed, as presented in Fig. 7. The other impregnated metal catalysts, Ni/AC, Pt/AC, and Pd/AC, suffered blocking at different degrees, as they failed to maintain specific surface area and pore volume. The Ni/AC and Pt/AC show similar patterns, as they lose specific surface area and pore volume but still maintain the average pore diameter. These could be explained by both catalysts suffering intermediate blocking from metal aggregation inside the pores that caused partial blockage.

On the other hand, Pd/AC catalyst showed an interesting phenomenon where the average pore diameter is increased after the impregnation process. The pore size distribution of the Pd/AC catalyst, presented in Fig. 8, showed that there is an increase in pore volume in the trimodal region of 2.62, 3.18, and 3.90 nm. This could only be caused by pore widening, as that the AC support material does not have pore size distribution in other sizes that can be blocked into the new trimodal region of Pd/AC porosity. The pore widening from the impregnation method occurred to Pd/AC due to the total pore blackening from Pd metal aggregation inside the pores. The Pd metal aggregate allegedly pushes the support wall structure, making the catalyst pores become wider, hence increasing the average pore diameter. On the other hand, NiPd metals only caused partial blockage at the mesopores region, 2.8 nm. The porosity, acidity, and metal dispersion of the catalyst will affect their hydrocracking performance.

Hydrocracking Application

Hydrocracking results using various catalysts are presented in Table 2. Thermal cracking was employed as a benchmark to assess catalytic activity. As expected, thermal cracking yielded the lowest amount of liquid fraction while producing a higher residual feed. The catalysts employed in this study have demonstrated their

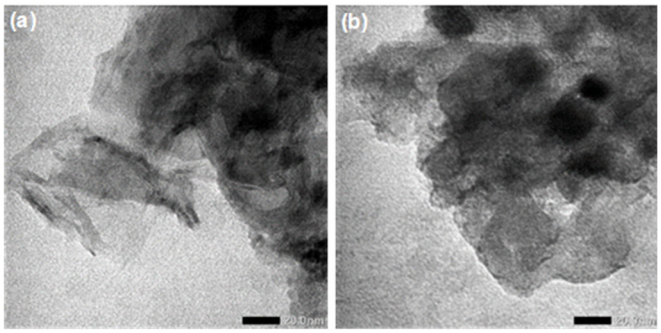

Fig 7. TEM images of fresh (a) and used (b) NiPd/AC catalyst

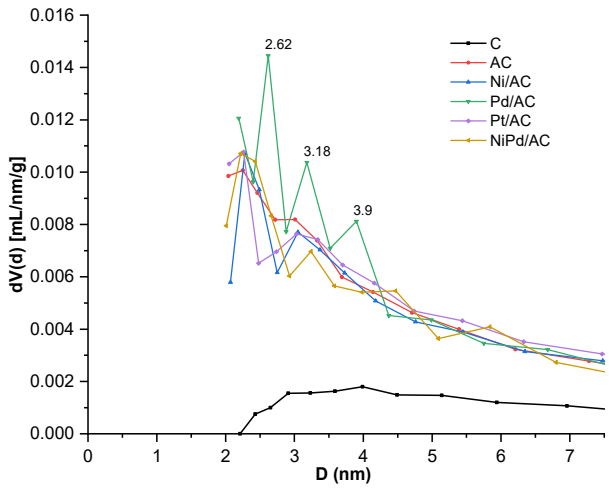

Fig 8. Pore size distribution of (a) C, (b) AC, (c) Ni/AC, (d) Pt/AC, (e) Pd/AC, and (f) NiPd/AC catalyst

Table 2. Catalyst performance testing on hydrocracking of castor oil

Catalyst	Product distribution (wt.%)				Selectivity in liquid product (wt.%)			
	Coke	Gas	Residue	Liquid	Gasoline	Diesel	Alcohol	Others
Thermal	0	20.85	1.39	77.76	4.78	0	56.66	16.32
AC	0.37	18.93	0.52	79.08	10.64	2.61	56.37	9.46
Ni/AC	0.38	18.05	0.18	81.39	11.21	2.85	61.36	5.97
Pt/AC	0.37	16.19	0.27	82.17	10.75	1.27	68.94	1.21
Pd/AC	0.24	17.19	0.46	83.11	11.34	0.72	68.95	2.10
NiPd/AC 1×	0.22	12.51	0.46	88.80	15.16	1.08	71.69	0.87
NiPd/AC 2×	0.42	16.26	0.85	82.48	11.58	0.69	65.85	4.35
NiPd/AC 3×	0.40	14.70	0.56	84.35	13.86	1.45	62.16	6.87

ability to enhance the conversion of castor oil into liquid fractions. However, the high ricinoleic acid content in castor oil poses challenges, as the primary objective of hydrocracking is to maximize hydrocarbon production. Consequently, the catalysts must possess essential hydrodeoxygenation and decarboxylation capabilities to effectively address this hurdle.

The observed liquid fraction appears to align with the theoretical acidity trend, wherein catalysts with more acid metal tend to yield a greater liquid fraction. The acidity value plays a significant role in the hydrocracking of castor oil, as it represents the availability of acid sites for the desired hydrocracking reactions. Both noble metal catalysts, Pt/AC and Pd/AC, exhibit similar behavior in terms of their liquid selectivity, indicating comparable hydrocracking performance between Pt and Pd metals. The observed variations between these catalysts can be attributed to differences in acidity and porosity properties inherent to each catalyst. Despite Pt/AC and Pd/AC yielding higher liquid fractions compared to the Ni/AC catalyst, they demonstrate slightly lower gasoline fractions. This suggests that the Ni metal in the Ni/AC system exhibits slightly better hydrodeoxygenation and/or decarboxylation activity than Pd and Pt metals despite its lower activity as reflected in the total liquid yield of Ni/AC. The superior performance of Ni/AC can be explained by the synergetic cooperation between the metal and support interactions, contributing to its overall superior quality.

The NiPd/AC catalyst exhibits notable synergetic cooperation, as evidenced by the efficient dispersion of Ni and Pd metals across the AC support, resulting in the catalyst's highest surface area among the metal-loaded catalysts. This synergetic cooperation also contributes to its exceptional hydrocracking performance. In comparison to other catalysts, the bimetallic catalyst demonstrates superior performance, characterized by the highest total liquid fraction and hydrocarbon fraction, while minimizing the formation of gas fraction. Remarkably, the hydrocracking product profile of the bimetallic catalyst differs significantly from that of the monometallic catalyst, which only marginally surpasses the support's performance. This outstanding performance is attributed to the combined effects of the high acidity value and the well-dispersed bimetallic system across the AC support. These two remarkable features inherent in the NiPd/AC catalyst result in high conversion and favorable selectivity. Consequently, this catalyst was selected for the reusability test, further evaluating its long-term performance and sustainability.

The catalyst reusability test data is provided in Table 2. Following each use of the catalyst, an increase in mass was observed due to the formation of coke on the catalyst surface. The accumulation of coke appears to hinder the hydrocracking function of the catalyst, as subsequent yields could not match the initial performance. Despite the catalyst's vulnerability to coke formation, it exhibits the ability to regenerate itself while maintaining its hydrocracking activity. This regenerative behavior is evident in the third cracking, where coke formation was less severe compared to the initial cracking, leading to improved liquid fraction yield and selectivity. Visual evidence of this regeneration process can be observed in TEM images provided in Fig. 7. Even after three consecutive hydrocracking cycles, the

dispersion of the bimetallic system across the AC support remains unaffected. In conclusion, the NiPd/AC catalyst retains favorable properties and performance for the hydrocracking of castor oil, underscoring its potential as a reliable catalyst for this process.

■ CONCLUSION

In this research, we found the optimum KOH impregnation ratio was 2:1, as it has the highest iodine value of 751.94 mg/g. We also found a synergetic interaction between Ni and Pd metal in the bimetallic dispersion across activated carbon and in the castor oil hydrotreating application. The liquid fraction yielded by NiPd/AC was 88.80 wt.%, with 15.16 wt.% as C5-C12 hydrocarbons, 71.69 wt.% as alcohol compounds, and only 0.87 wt.% still as organic compounds. The NiPd/AC catalyst performance was not significantly dropped after being reused, which indicates that coking in NiPd/AC does not alter much of its active sites.

■ ACKNOWLEDGEMENTS

The authors would like to thank Universitas Gadjah Mada for the research facility and instrumentation.

■ AUTHOR CONTRIBUTIONS

Wega Trisunaryanti did the conceptualization, supervision, resources, methodology, writing – review, editing, and funding acquisition. Triyono and Iip Izul Falah did methodology and validation. Dwi Bagus Wicaksono did the investigation, methodology, formal analysis, and visualization. Satriyo Dibyo Sumbogo did formal analysis, visualization, and writing - original draft.

■ REFERENCES

[1] Pleyer, O., Kubičková, I., Vráblík, A., Maxa, D., Pospíšil, M., Zbuzek, M., Schlehöfer, D., and Straka, P., 2022, Hydrocracking of heavy vacuum gas oil with petroleum wax, *Catalysts*, 12 (4), 384.

[2] Ward, J.W., Michalek, J.J., Azevedo, I.L., Samaras, C., and Ferreira, P., 2019, Effects of on-demand ridesourcing on vehicle ownership, fuel consumption, vehicle miles traveled, and emissions per capita in US States, *Transp. Res. Part C: Emerging Technol.*, 108, 289–301.

[3] Mathew, G.M., Raina, D., Narisetty, V., Kumar, V., Saran, S., Pugazhendi, A., Sindhu, R., Pandey, A., and Binod, P., 2021, Recent advances in biodiesel production: Challenges and solutions, *Sci. Total Environ.*, 794, 148751.

[4] Jamil, F., Al-Haj, L., Al-Muhtaseb, A.H., Al-Hinai, M.A., Baawain, M., Rashid, U., and Ahmad, M.N.M., 2018, Current scenario of catalysts for biodiesel production: A critical review, *Rev. Chem. Eng.*, 34 (2), 267–297.

[5] Hasanudin, H., Asri, W.R., Said, M., Hidayati, P.T., Purwaningrum, W., Novia, N., and Wijaya, K., 2022, Hydrocracking optimization of palm oil to bio-gasoline and bio-aviation fuels using molybdenum nitride-bentonite catalyst, *RSC Adv.*, 12 (26), 16431–16443.

[6] Wijaya, K., Saputri, W.D., Aziz, I.T.A., Wangsa, W., Heraldy, E., Hakim, L., Suseno, A., and Utami, M., 2022, Mesoporous silica preparation using sodium bicarbonate as template and application of the silica for hydrocracking of used cooking oil into biofuel, *Silicon*, 14 (4), 1583–1591.

[7] Lin, M., Zhang, X., Zhan, L., Li, X., Song, X., and Wu, Y., 2022, Product distribution-tuned and excessive hydrocracking inhibiting in fatty acid deoxygenation over amorphous Co@SiO_2 porous nanorattles, *Fuel*, 318, 123605.

[8] Salamah, S., Trisunaryanti, W., Kartini, I., and Purwono, S., 2022, Synthesis of mesoporous silica from beach sand by sol-gel method as a Ni supported catalyst for hydrocracking of waste cooking oil, *Indones. J. Chem.*, 22 (3), 726–741.

[9] Roy, P., Jahromi, H., Rahman, T., Adhikari, S., Feyzbar-Khalkhali-Nejad, F., Hassan, E.B., and Oh, T.S., 2022, Understanding the effects of feedstock blending and catalyst support on hydrotreatment of algae HTL biocrude with non-edible vegetable oil, *Energy Convers. Manage.*, 268, 115998.

[10] Alisha, G.D., Trisunaryanti, W., and Syoufian, A., 2022, Mesoporous silica from Parangtritis beach sand templated by CTAB as a support of Mo Metal as a catalyst for hydrocracking of waste palm cooking oil into biofuel, *Waste Biomass Valorization*, 13 (2), 1311–1321.

[11] Janampelli, S., and Darbha, S., 2019, Hydrodeoxygenation of vegetable oils and fatty acids over different group VIII metal catalysts for producing biofuels, *Catal. Surv. Asia*, 23 (2), 90–101.

[12] Di Vito Nolfi, G., Gallucci, K., and Rossi, L., 2021, Green diesel production by catalytic hydrodeoxygenation of vegetables oils, *Int. J. Environ. Res. Public Health*, 18 (24), 13041.

[13] Liu, S., Simonetti, T., Zheng, W., and Saha, B., 2018, Selective hydrodeoxygenation of vegetable oils and waste cooking oils to green diesel using a silica-supported Ir–ReOx bimetallic catalyst, *ChemSusChem*, 11 (9), 1446–1454.

[14] Yeboah, A., Ying, S., Lu, J., Xie, Y., Amoanimaa-Dede, H., Boateng, K.G.A., Chen, M., and Yin, X., 2021, Castor oil (*Ricinus communis*): A review on the chemical composition and physicochemical properties, *Food Sci. Technol.*, 41, 399–413.

[15] Liu, S., Zhu, Q., Guan, Q., He, L., and Li, W., 2015, Bio-aviation fuel production from hydroprocessing castor oil promoted by the nickel-based bifunctional catalysts, *Bioresour. Technol.*, 183, 93–100.

[16] Trisunaryanti, W., Triyono, T., Purwono, S., Purwanti, A.S., and Sumbogo, S.D., 2022, Synthesis of mesoporous carbon from merbau sawdust as a nickel metal catalyst support for castor oil hydrocracking, *Bull. Chem. React. Eng. Catal.*, 17 (1), 216–224.

[17] Alvarez-Galvan, M.C., Campos-Martin, J.M., and Fierro, J.L., 2019, Transition metal phosphides for the catalytic hydrodeoxygenation of waste oils into green diesel, *Catalysts*, 9 (3), 293.

[18] Zharova, P.A., Chistyakov, A.V., Shapovalov, S.S., Pasynskii, A.A., and Tsodikov, M.V., 2019, Original Pt-Sn/Al_2O_3 catalyst for selective hydrodeoxygenation of vegetable oils, *Energy*, 172, 18–25.

[19] Yurpalov, V.L., Neponiashchii, A.A., Drozdov, V.A., Antonicheva, N.V., Buluchevskiy, E.A., and Lavrenov, A.V., 2021, The deactivation of acidic sites of NiMo/B_2O_3–Al_2O_3 catalysts during vegetable oil hydrodeoxygenation studied by EPR spectroscopy, *Magn. Reson. Chem.*, 59 (6), 600–607.

[20] Adams, B.D., and Chen, A., 2011, The role of palladium in a hydrogen economy, *Mater. Today*, 14 (6), 282–289

[21] Pal, N., Verma, V., Khan, A., Mishra, A., Anand, M., Venkata Pramod, C., Akhtar Farooqui, S., and Kumar Sinha, A., 2022, Hydrotreating and hydrodemetalation of raw jatropha oil using mesoporous Ni-Mo/γ-Al_2O_3 catalyst, *Fuel*, 326, 125108.

[22] Trisunaryanti, W., Sumbogo, S.D., Mukti, R.R., Kartika, I.A., Hartati, H., and Triyono, T., 2021, Performance of low-content Pd and high-content Co, Ni supported on hierarchical activated carbon for the hydrotreatment of *Calophyllum inophyllum* oil (CIO), *React. Kinet., Mech. Catal.*, 134 (1), 259–272.

[23] Trisunaryanti, W., Suarsih, E., Triyono, T., and Falah, I.I., 2019, Well-dispersed nickel nanoparticles on the external and internal surfaces of SBA-15 for hydrocracking of pyrolyzed α-cellulose, *RSC Adv.*, 9 (3), 1230–1237.

[24] Robinson, A.M., 2016, The Role of Oxophilic Metal Promoters in Bimetallic Hydrodeoxygenation Catalysts, *Dissertation*, University of Colorado at Boulder.

[25] Trisunaryanti, W., Sumbogo, S.D., Novianti, S.A., Fatmawati, D.A., Ulfa, M., and Nikmah, Y.L., 2021, ZnO-Activated carbon blended as a catalyst for oxidative desulfurization of dibenzothiophene, *Bull. Chem. React. Eng. Catal.*, 16 (4), 881–887.

[26] Oginni, O., Singh, K., Oporto, G., Dawson-Andoh, B., McDonald, L., and Sabolsky, E., 2019, Effect of one-step and two-step H_3PO_4 activation on activated carbon characteristics, *Bioresour. Technol. Rep.*, 8, 100307.

[27] Yang, W., and Liu, Y., 2021, Removal of Elemental Mercury using seaweed biomass-based porous carbons prepared from microwave activation and H_2O_2 modification, *Energy Fuels*, 35 (3), 2391–2401.

[28] Demir, M., and Doguscu, M., 2022, Preparation of porous carbons using NaOH, K_2CO_3, Na_2CO_3 and $Na_2S_2O_3$ activating agents and their supercapacitor application: A comparative study, *ChemistrySelect*,

7 (4), e202104295.

[29] Bag, O., Tekin, K., and Karagoz, S., 2020, Microporous activated carbons from lignocellulosic biomass by KOH activation, *Fullerenes, Nanotubes Carbon Nanostruct.*, 28 (12), 1030–1037.

[30] Chen, R., Li, L., Liu, Z., Lu, M., Wang, C., Li, H., Ma, W., and Wang, S., 2017, Preparation and characterization of activated carbons from tobacco stem by chemical activation, *J. Air Waste Manage. Assoc.*, 67 (6), 713–724.

[31] Liang, Q., Liu, Y., Chen, M., Ma, L., Yang, B., Li, L., and Liu, Q., 2020, Optimized preparation of activated carbon from coconut shell and municipal sludge, *Mater. Chem. Phys.*, 241, 122327.

[32] Saab, R., Polychronopoulou, K., Zheng, L., Kumar, S., and Schiffer, A., 2020, Synthesis and performance evaluation of hydrocracking catalysts: A review, *J. Ind. Eng. Chem.*, 89, 83–103.

[33] Oginni, O., Singh, K., Oporto, G., Dawson-Andoh, B., McDonald, L., and Sabolsky, E., 2019, Influence of one-step and two-step KOH activation on activated carbon characteristics, *Bioresour. Technol. Rep.*, 7, 100266.

[34] Djilani, C., Zaghdoudi, R., Djazi, F., Bouchekima, B., Lallam, A., Modarressi, A., and Rogalski, M., 2015, Adsorption of dyes on activated carbon prepared from apricot stones and commercial activated carbon, *J. Taiwan Inst. Chem. Eng.*, 53, 112–121.